

## Electronic Supplementary Information

### Large-Scale Low –Temperature Fabrication of SnO<sub>2</sub> Hollow/Nanoporous

### Nanostructures: Template-Engaged Replacement Reaction Mechanism and

### High-Rate Lithium Storage

*Yuan-Li Ding, Yuren Wen, Peter A. van Aken, Joachim Maier, and Yan Yu\**

[\*] Prof. Y. Yu

CAS Key Laboratory of Materials for Energy Conversion, Department of Materials Science and Engineering, University of Science and Technology of China, Hefei, 230026, Anhui, P. R. China

E-mail: [yanyumse@ustc.edu.cn](mailto:yanyumse@ustc.edu.cn)

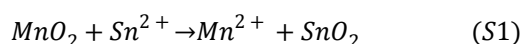
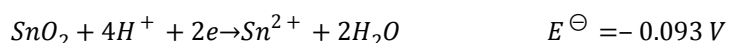
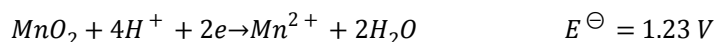
Dr. Y. L. Ding, Prof. J. Maier, Prof. Y. Yu

Max Planck Institute for Solid State Research, Heisenbergstrasse 1, 70569, Stuttgart, Germany

Dr. Y. R. Wen, Prof. P. A. van Aken

Max Planck Institute for Intelligent Systems, Heisenbergstrasse 3, 70569, Stuttgart, Germany

### The thermodynamic analyses of the redox reaction between MnO<sub>2</sub> and Sn<sup>2+</sup>.



Nernst equation: 
$$E_{\text{cell}} = E_{\text{cell}}^\ominus - \frac{RT}{nF} \ln \frac{[\text{Mn}^{2+}]}{[\text{Sn}^{2+}]} \quad (\text{S2})$$

$E_{cell}^{\ominus}$ : standard cell potential

$E_{cell}$ : cell potential at the temperature of interest

R: universal gas constant,  $R=8.314 \text{ J K}^{-1} \text{ mol}^{-1}$

T: absolute temperature

n: the number moles of electron transferred in the half-cell reaction

F: Faraday constant,  $F=96485 \text{ C mol}^{-1}$

Generally, the ion activities in the Nernst equation are replaced by concentrations.

It is assumed that the ratios of  $[\text{Mn}^{2+}]/[\text{Sn}^{2+}]$  are 1:999 (when the cell is activated) and 999:1 (when the cell reaction finishes), respectively. The actual cell potentials are as follows according to Nernst equation (80 °C).

$$E_{\text{initial}} = 1.43 \text{ V}$$

$$E_{\text{end}} = 1.22 \text{ V}$$

$$\Delta G = -nEF \quad (S3)$$

According to Equation S3, “ $\Delta G_{\text{initial}} = -275.95 \text{ kJ}$ ” reveals that the redox reaction is a exergonic process when  $E_{\text{initial}}$  equals 1.43 V. Even at room temperature, the redox reaction between  $\text{MnO}_2$  and  $\text{Sn}^{2+}$  ions can occur but requires a relatively long time (2 or 3 days).

As shown in scheme S1, the radius ( $r$ ) of SO-NT equals 1.5  $R$  ( $R$ : the radius of MO-NR). The detailed calculation is as follows. We assumed that the length of SO-NT after the transformation keeps no change.

$$V_{\text{MnO}_2} = n_{\text{MnO}_2} \cdot V_{M(\text{MnO}_2)} \quad (S4)$$

$$V_{SnO_2} = n_{SnO_2} \cdot V_{M(SnO_2)} \quad (S5)$$

$V_{M(MnO_2)}$ : Molar volume of  $MnO_2$ ,  $17.28 \text{ cm}^3 \text{ mol}^{-1}$ .

$V_{(MnO_2)}$ : Volume of MO-NR.

$V_{M(SnO_2)}$ : Molar volume of  $SnO_2$ ,  $21.68 \text{ cm}^3 \text{ mol}^{-1}$ .

$V_{SnO_2}$ : Volume of SO-NT.

According to Equation (S1),  $n_{SnO_2}$  should equal  $n_{MnO_2}$  after redox reaction.

$$V_{SnO_2} = \frac{V_{M(SnO_2)}}{V_{M(MnO_2)}} V_{MnO_2}$$

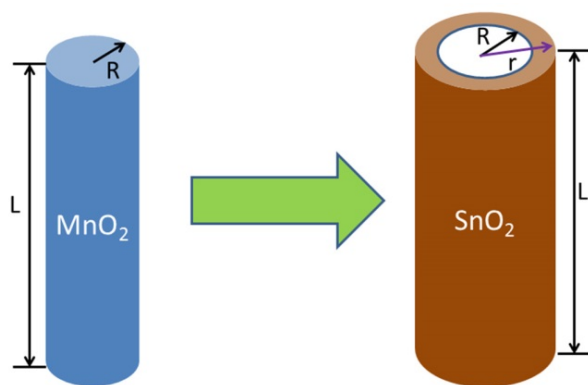
Ignoring porosity, we conclude that

During the transformation,  $SnO_2$  nanograins prefer outward growth along the MO-NR walls. Thus, we assume the volume of interior hollow space in SO-NT to be almost the same as  $V_{MnO_2}$ .

$$V_{total} = V_{MnO_2} + V_{SnO_2} = \left(1 + \frac{V_{M(SnO_2)}}{V_{M(MnO_2)}}\right) V_{MnO_2} \quad (S6)$$

Based on the volume ratio of MO-NR and SO-NT (Scheme S1), we conclude

$r = \sqrt{1 + (V_{M(SnO_2)})/(V_{M(MnO_2)})}$   $R=1.5$  R. As this is well fulfilled, in spite of the porosity of  $SnO_2$ , we conclude that the pore volume is compensated by the  $SnO_2$  particles in the interior.



**Scheme S1.** The schematic illustration from MO-NR to SO-NT, R and r represent the radii of MO-NR and SO-NT, respectively. The length of MO-NR is assumed to keep no change after the redox transformation.

#### **Urchin-like SnO<sub>2</sub> (SO-U) prepared by template-engaged replacement reaction.**

The urchin-like morphology of the template can be well retained after the redox reaction. Compared to urchin-like  $\alpha$ -MnO<sub>2</sub> (the diameter of each nanorod is 50-70 nm), the diameter of each nanotube in SO-U is increased to 80-110 nm, suggesting the outward growth of SnO<sub>2</sub> nanograins. The resulting SO-U also consists of numerous nanotubes with closed ends. Some nanorods with opened ends can be observed from some broken products marked by arrows in Figure 2b, which is clearly observed from the samples after calcination at 600 °C (Figure S8), implying that the ends of nanorods in the SO-U are not robust enough compared to the walls of the products. HRTEM image shows that the walls of nanotubes in SO-U are porous and composed of nanoparticles with a size of 5-15 nm (Figure S7b). Lattice fringes assigned to (110) plane of tetragonal SnO<sub>2</sub> are clearly seen (Figure S7d), revealing a well-defined lattice order of SO-U.

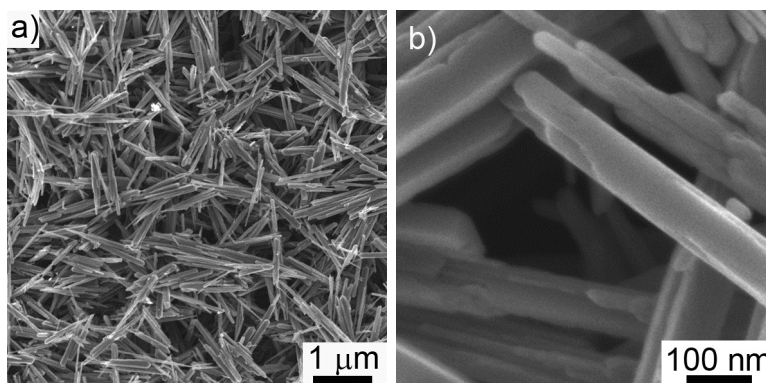


**Figure S1.** SEM images of a) low-magnification and b) high-magnification  $\beta$ -MnO<sub>2</sub> nanorods.

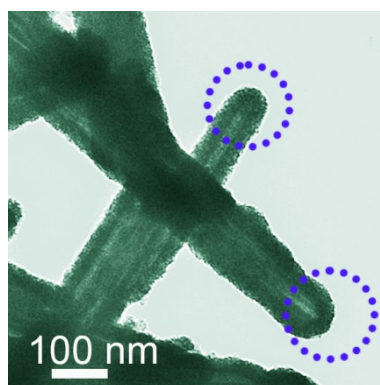


**Figure S2.** TEM image of SO-NT with closed ends marked by the dotted circles.

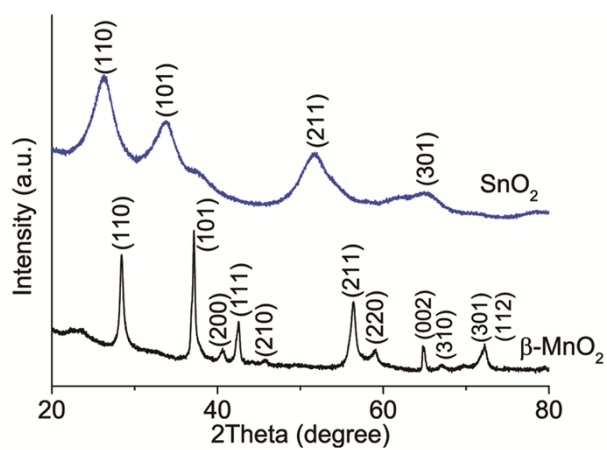


**Figure S3.** XRD patterns of  $\beta$ -MnO<sub>2</sub> nanorods and SO-NT.

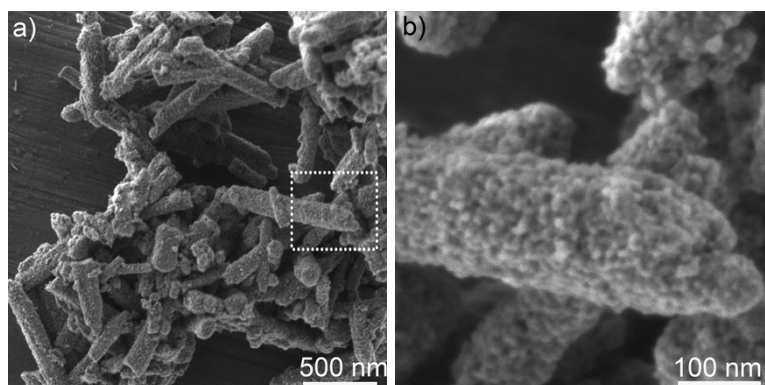


**Figure S4.** SEM images of a) SO-NT after calcination at 600 °C, b) the magnified view corresponding to the boxed area in (a).

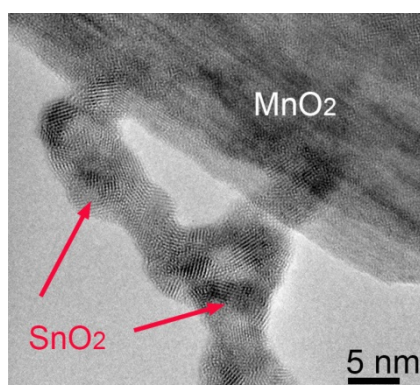


**Figure S5.** HRTEM image of the intermediate product at the initial reaction stage between  $\beta$ -MnO<sub>2</sub> nanorods and Sn<sup>2+</sup>.

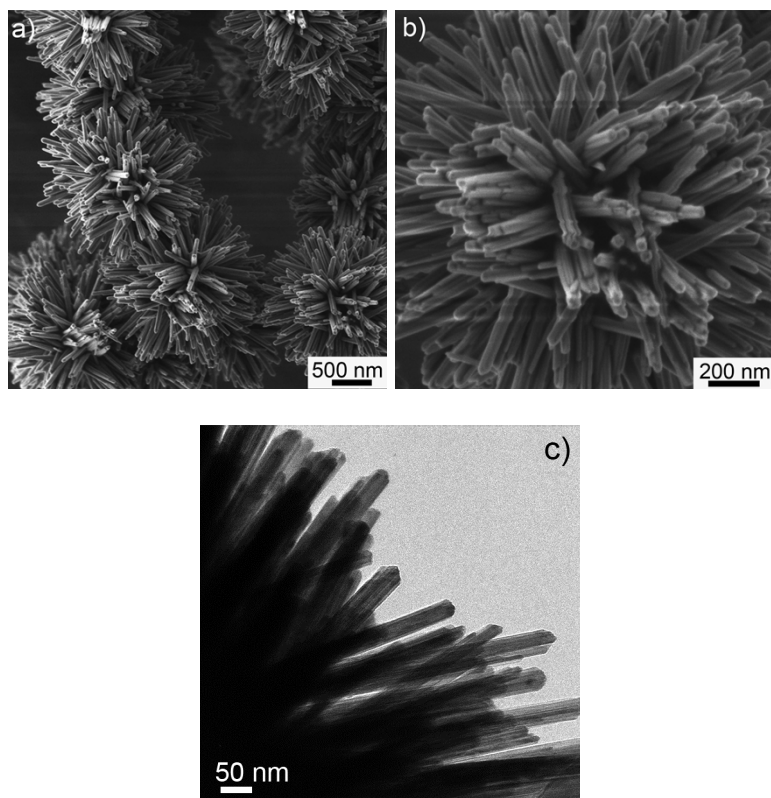


**Figure S6.** a, b) SEM images and c) TEM image of urchin-like  $\alpha$ - $\text{MnO}_2$ .

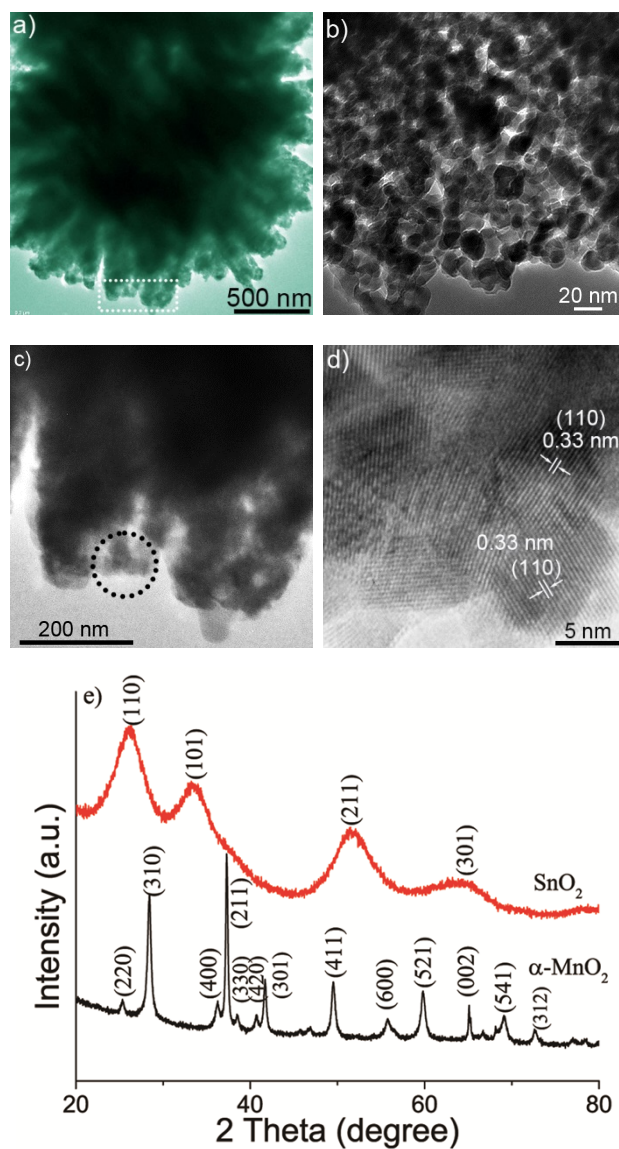


**Figure S7.** a) TEM image of SO-U, b) high-magnification TEM image of the tip of an individual nanotube in SO-U, c) the view taken from the boxed area in (a), d) HRTEM image taken from the circled area in (c). e) XRD patterns of the resulting urchin-like  $\alpha$ - $\text{MnO}_2$  and  $\text{SnO}_2$ .



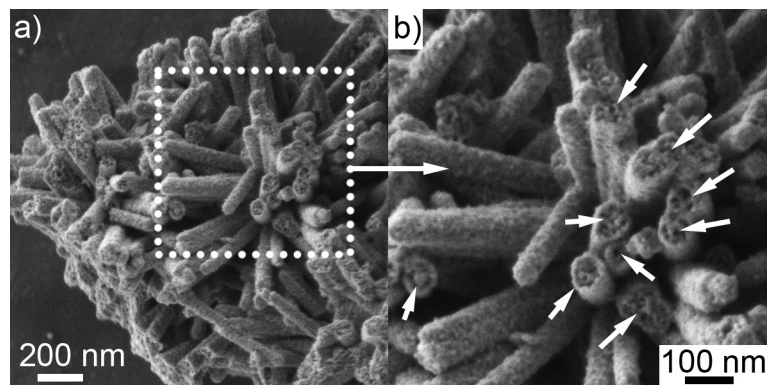


**Figure S8.** SEM images of a) SO-U after calcination at 600 °C, b) the magnified view corresponding to the boxed area in (a). The arrows indicate the formation of open ends for individual nanotubes after calcination at 600 °C.

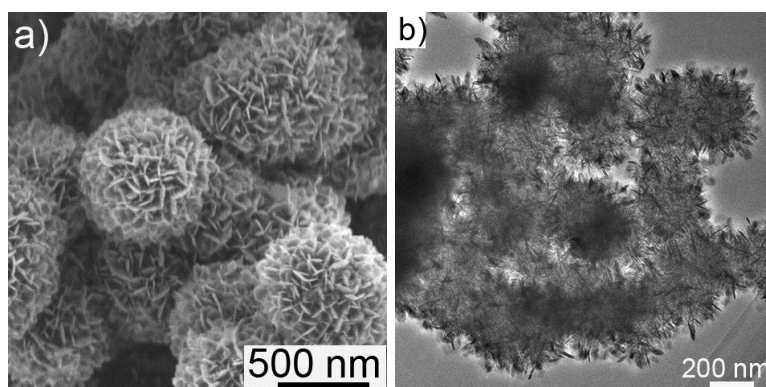


**Figure S9.** a) SEM and b) TEM images of  $\epsilon$ -MnO<sub>2</sub> nanospheres.

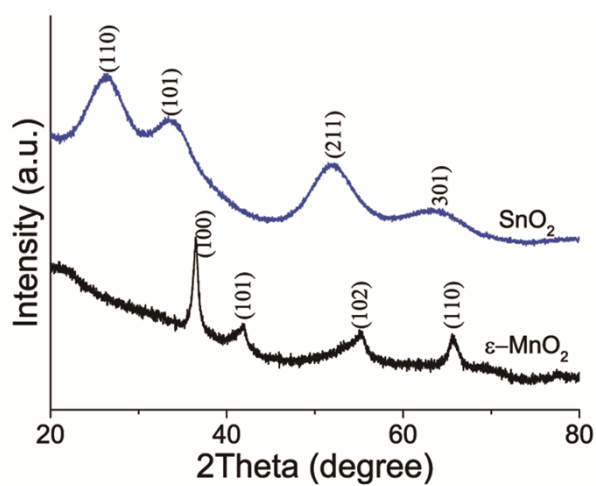


**Figure S10.** XRD patterns of  $\epsilon$ -MnO<sub>2</sub> and SO-NS.

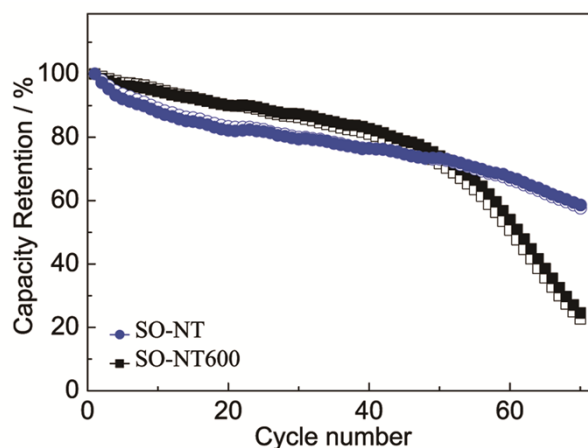


**Figure S11.** The comparison of cycling stability at  $1 \text{ A g}^{-1}$  between SO-NT (blue symbols) and SO-NT600 (black symbols) after calcination at  $600^\circ\text{C}$ . The solid and empty symbols represent the discharge and charge capacities, respectively.

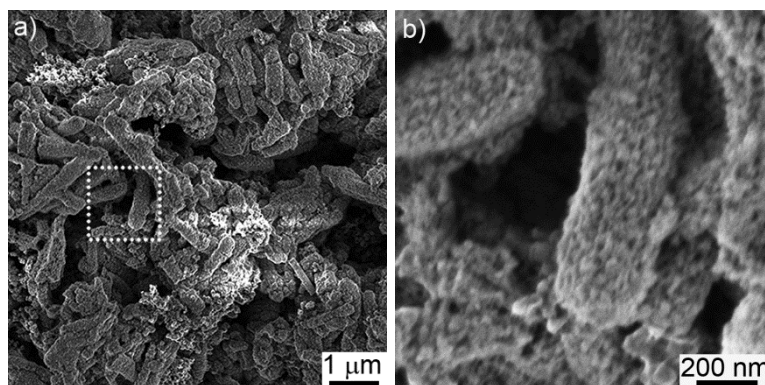


**Figure S12.** SEM images of a) SO-NT electrode after 60 cycles at  $0.5 \text{ A g}^{-1}$ , b) the magnified view corresponding to the boxed area in (a).

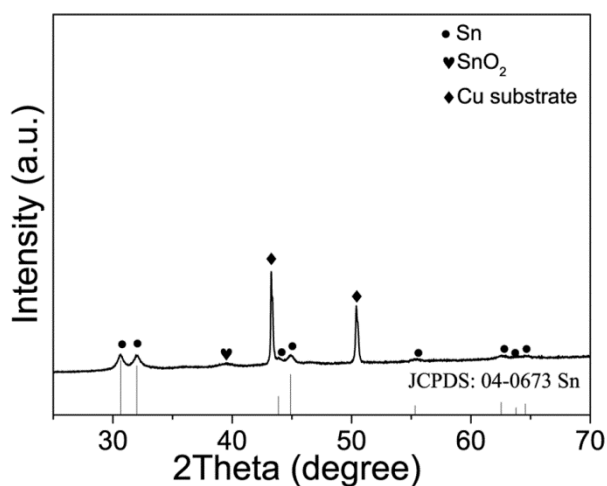


**Figure S13.** XRD pattern of SO-NT electrode after 60 cycles at  $0.5 \text{ A g}^{-1}$ .